

Quantitative analysis of aluminum samples in He ambient gas at different pressures in a thick LIBS plasma

Fatemeh Rezaei¹ · Seyed Hassan Tavassoli²

Received: 9 April 2015 / Accepted: 27 June 2015 / Published online: 16 July 2015
© Springer-Verlag Berlin Heidelberg 2015

Abstract In this paper, the influences of He ambient gas on aluminum emissions are investigated by experimental analysis of LIBS spectrum. Plasma is produced by focusing of a Nd:YAG laser pulse at a wavelength of 1064 nm on Al standard samples. In this work, the effects of helium atmosphere at different pressures on the amount of spectral self-absorption are studied. The results are discussed by utilizing two approaches: the curve of growth and calibration curve. It is seen that by increasing the gas pressure, the self-absorption enhances. Also, a new method of applying one standard sample instead of other traditional techniques is introduced for concentration prediction. The presented method would be helpful for the situation in which supplying standard samples is not very easy. Then, the accuracy of this new method can be checked by comparison of concentration prediction of the standard samples with their real concentrations.

1 Introduction

In recent years, studying on laser-induced breakdown spectroscopy (LIBS) has been increased due to its expanding applications in geological material [1–8], cultural heritage [9–13], works of art [14–18], environmental monitoring

(radioactive, high temperature, toxic materials) [19–25], industry [26–31], architecture, medical (noninvasive study of human teeth and hair, diagnosis of cancer tissue, DNA analysis) [32–37], military and civil security (detection of explosive material and biological weapons) [38–43]. Most of these applications are investigated under the condition of earth's atmosphere (i.e., at 760 Torr in air atmosphere) in order to determine the selected material compositions. Nevertheless, interest in LIBS in other ambient gases with various circumstances has been grown because of its practical application. It should be mentioned that nowadays wide applications of gas effects in space exploration (such as utilizing LIBS for investigating specific conditions on Venus and Mars) [4, 44, 45] are studied. For instance, in scope of gas pressure, the high-pressure environment serves to replicate the conditions of a nuclear reactor or simulate some planet environments [46]. At the opposite, reduced gas pressures or vacuum is applied for determination of isotope ratios [47–49], synthesis of nanoparticles and thin films.

Different research groups [50–55] have investigated the quantitative analysis of plasma parameters and spectral line properties in LIBS technique by considering the influences of gas conditions. For instance, Effenberger et al. [56] have properly presented a review of applications of different gas effects in LIBS experiment. They have comprehensively mentioned the results of various groups about the effects of atmosphere compositions and gas pressures (higher and lower than 760 Torr) on plasma parameters and spectral line characteristics. Dawood et al. [57] have investigated the effects of gas nature and its pressure on temporal distribution of aluminum plasma. They have explained that both plasma temperature and electron density grow with ambient gas pressure. In addition, they have shown that argon provides the highest temperature and plasma density, helium provides the lowest one, and nitrogen produces

✉ Fatemeh Rezaei
fatemehrezaei@kntu.ac.ir
Seyed Hassan Tavassoli
h-tavassoli@sbu.ac.ir

¹ Department of Physics, Khaje Nasir Toosi University of Technology, 15875-4416 Shariati, Tehran, Iran

² Laser and Plasma Research Institute, Shahid Beheshti University, G. C., 1983963113 Evin, Tehran, Iran

intermediate mentioned parameters. Farid et al. [58] have studied the influences of ambient gases of air, argon and helium at different pressures on laser-induced copper plasma and its surface morphology. They have obtained the optimized experimental condition (the pressure and nature of ambient gas) for determination of electron temperature, spectral emission intensity and plasma species densities. Furthermore, Iida [52] has comprehensively studied the effects of different ambient gases on laser excitation and evaporation process by spectral analysis. She has investigated the variation of plasma parameters such as electron density and plasma temperature in Ar, air and He gases at different pressures. She has explained a discussion on possibility of occurring gas breakdown before sample vaporization and alteration in couple of laser irradiation to the sample surface. It should be noted that for completing of the results, some research groups have investigated the influences of laser characteristics on spectral emissions in the presence of different surrounding gases. For example, Lee et al. [59] have studied the effects of laser wavelength on copper plasma emissions by using Q-switched Nd:YAG (at 532 and 1064 nm) and excimer laser (at 308 nm) in He, Ar and Ne atmosphere. They have found that under excimer laser irradiation, self-absorption effects were seen in a helium atmosphere at different gas pressures, while intermediate self-absorption was observed in neon atmosphere and self-absorption occurred in argon noble gas only at low gas pressures.

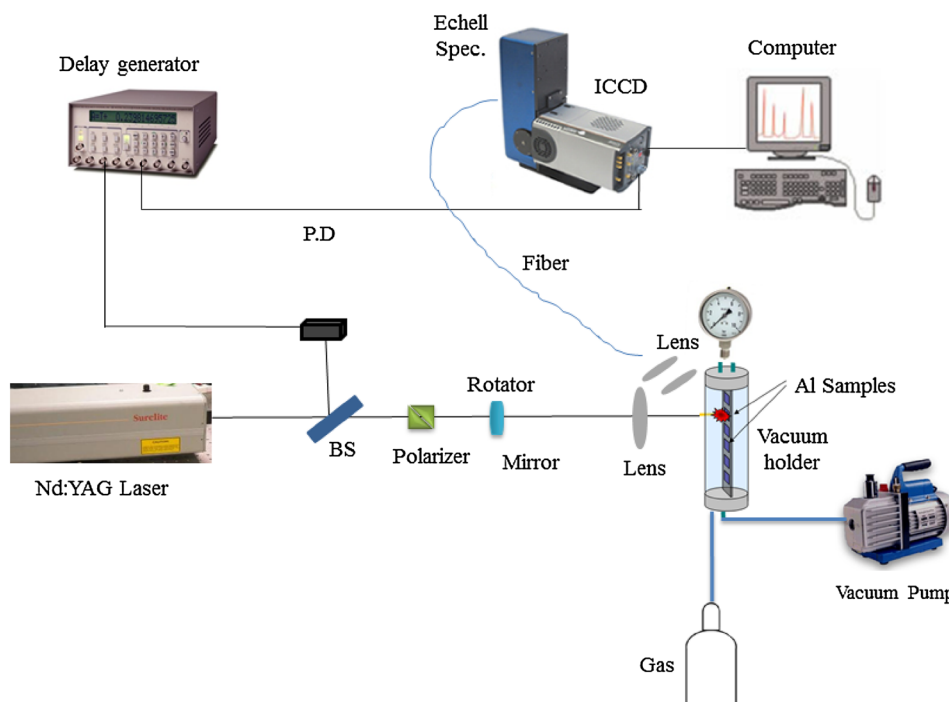
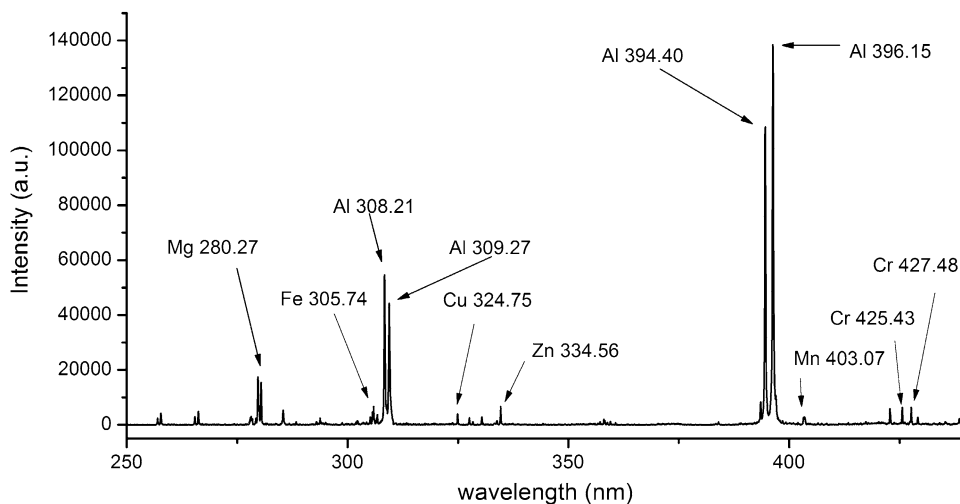
It should be mentioned that in spectral analysis, self-absorption is an important phenomenon, especially at high concentrations, which causes remarkable errors in quantitative evaluation of sample compositions. Self-absorption is noticeable for spectral lines with high-transition probabilities or atomic lines with low excitation energies of the upper levels. Furthermore, resonant lines are essentially affected by the self-absorption phenomenon. Therefore, self-absorption must be completely corrected for exact quantitative analysis. Different groups corrected this effect by several experimental and theoretical methods [60, 61] of duplicating mirror [62], line ratio [63], curve of growth [64–68], calibration free [69, 70] and fitting algorithms [71, 72] for performing the accurate analysis. For instance, Cristoforetti et al. [63, 73] estimated the self-absorption coefficient by considering the ratio of different parameters such as spectral peak intensity, line width, as well as integrated intensity of a specific spectral line in the case of experimental condition (with self-absorption) to the case of thin plasma (without self-absorption). In previous study of our group [74], the effects of noble gases of He and Ar at 1 atm pressure on laser-induced plasma emission of aluminum sample were investigated. Moreover, a comparison between thin and thick aluminum radiation was carried out. In addition, the self-absorption coefficient of each aluminum

strong line under different laser energies was estimated. So, in the present study, for the completeness of the results, the gas pressure effects from atmospheric to a few Torr on the magnitude of spectrum self-absorption are studied by utilizing the appropriate experimental setup. A comparison of the results is quantitatively given by two techniques: experimental curve of growth and calibration curve. Also, a new method of using one standard sample is introduced for quantitative analysis for the cases of special situations with limited standard samples. Then, the accuracy of the presented model can be checked with standard samples with known concentrations.

2 Experimental setup

A schematic of the experimental setup for studying of the gas effects on LIBS spectrum is shown in Fig. 1. A Q-switched Nd:YAG (yttrium aluminum garnet) laser with 10-ns pulse width and 10-Hz repetition rate is focused on the sample surface. In this experiment, laser energy is 100 mJ/pulse. Moreover, the focusing spot of laser is about 0.4 mm, and the laser irradiance on the target is around 2×10^{13} W/m². Six aluminum standard samples are located in a quartz tube (as a chamber) composed of the noble gas of helium. The chamber is connected to a vacuum pump in order to clean the tube space and is accompanied by a gauge for controlling the gas pressure. Here, He is chosen as the ambient gas due to its high thermal conductivity, causing smooth behavior in spectral lines. The samples inside the tube are placed on a rail so that their positions are changed by XYZ motion stage. XYZ moves the samples to face with fresh surfaces at each laser pulse. In this paper, He gas at different pressures of 0.11, 0.8, 8, 80 and 760 Torr is used for investigating the variations of spectral lines self-absorption. As it is seen in this figure, for time-resolved analysis, at a specific delay time, a beam splitter divides the laser pulse into two parts. One part is sent to a photodiode to trig a delay generator. The delay generator trigs the ICCD by sending a pulse to it. The other part of laser beam is passed through a rotator and a Glan–Taylor prism (polarizer) in order to adjust the laser energy. This laser pulse is irradiated perpendicularly on the samples and is focused by a quartz lens to create the plasma in front of the Al samples. The plasma emission is collected by another quartz lens with 4 cm focal length, which is accompanied by an objective lens with 2 cm focal length. Then, the radiation is transmitted from the objective lens to an optical fiber which guides the plasma emissions to an echelle spectrograph (with 0.02-nm spectral resolution) which is equipped by an intensified charge-coupled (ICCD) camera. Here, the real spectral resolution, including the intensifier effect is 0.2 nm.

In this experiment, each recorded spectrum is an accumulation of three consecutive laser shots. Furthermore,

Fig. 1 Diagram of LIBS experimental setup**Fig. 2** Typical spectrum of Al at 2- μ s delay time and at 1 atm pressure

by repetition of the experiment at different delay times, the optimum acquisition delay and acquisition time are chosen as 2 and 10 μ s, respectively. A typical spectrum of Al at 2- μ s delay time and at 1 atm pressure is shown in Fig. 2. The characteristics of the observed spectral lines are inserted in Table 1. The data in Table 1 are extracted from NIST database [75].

3 Results and discussion

Generally, LIBS spectral emissions and its erosion due to self-absorption are widely affected by the implementation

conditions such as laser features like its energy, laser wavelength and pulse duration, as well as the surrounding gas characteristics. In this study, in below sections, the effects of He gas pressures are represented by time-resolved analysis which straightly influences on the quantitative measurements.

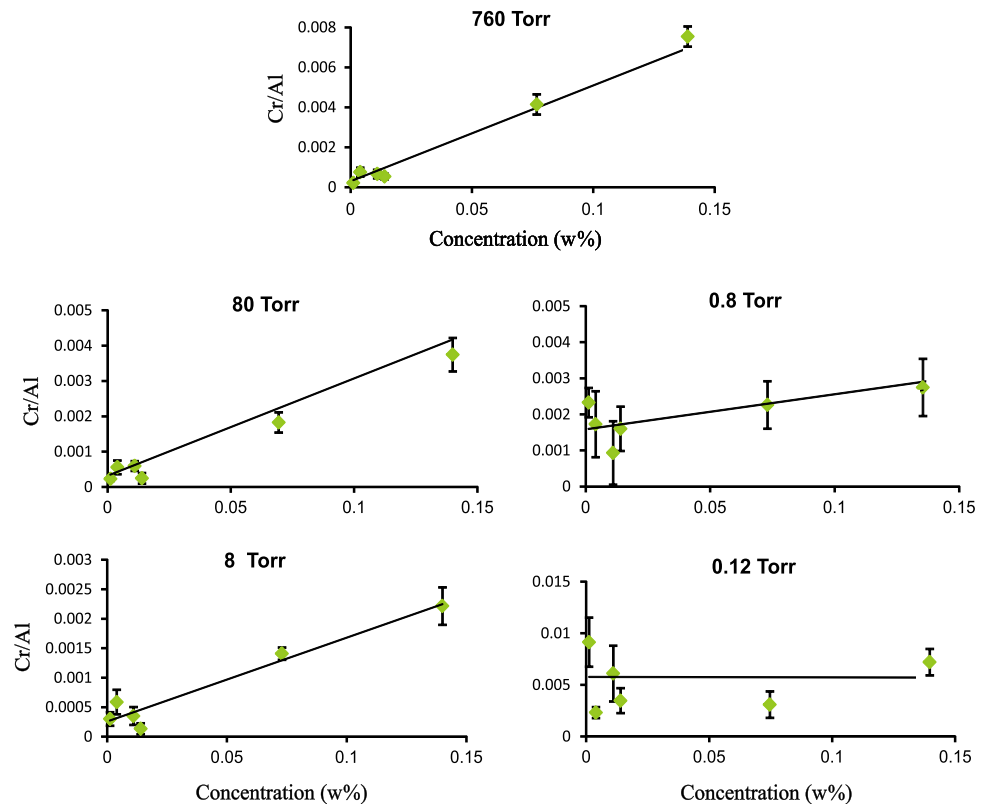
3.1 Self-absorption effect

In the previous work of our group, it was shown that the aluminum spectral lines in argon ambient gas are exposed to more intense self-absorption than in helium noble gas at the mentioned experimental condition [74]. So, since our results on the influences of gas natures on the plasma

Table 1 Spectral data of the different observed spectral lines of aluminum sample from NIST database [75] for evaluation of self-absorption

Element	λ_0 (nm)	$A \times 10^7$ (s ⁻¹)	$Ei \times 10^{-17}$ (J)	$Eu \times 10^{-17}$ (J)	g_u
Al I	257.5094	2.8	0.0022	0.0775	6
	308.2153	6.3	0	0.0645	4
	309.2710	7.4	0.0002	0.0645	6
	394.4006	4.93	0	0.0504	2
	396.1520	9.8	0.0002	0.0504	2
Mg II	280.2706	26	0	0.0708	2
Cu I	324.7540	13.9	0	0.0611	4
	327.3960	13.7	0	0.0607	2
Cr I	425.4332	3.15	0	0.0467	9
	427.4796	3.07	0	0.0465	7
Mn I	403.0753	1.7	0	0.0493	8
Zn I	334.5570	4	0.0653	0.1247	5
Fe I	305.7446	4.4	0.0138	0.0787	9

Fig. 3 Calibration curve of Cr spectral line at 427.48 nm and at different gas pressures of 0.12, 0.8, 8, 80 and 760 Torr



radiations are inserted in Refs. [74, 76], as well as for having smoother spectrum, the analysis in this paper is limited to Al samples in He noble gas. In addition, it should be noted that the details of the influences of the ambient gas natures at different pressure conditions are investigated in Refs. [52, 56, 59]. Hence, here, the effects of He ambient gas at different pressures of 0.11, 0.8, 8, 80 and 760 Torr on spectral self-absorption are investigated by two approaches: curve of growth and calibration curve.

3.2 Results of analysis with calibration curve approach

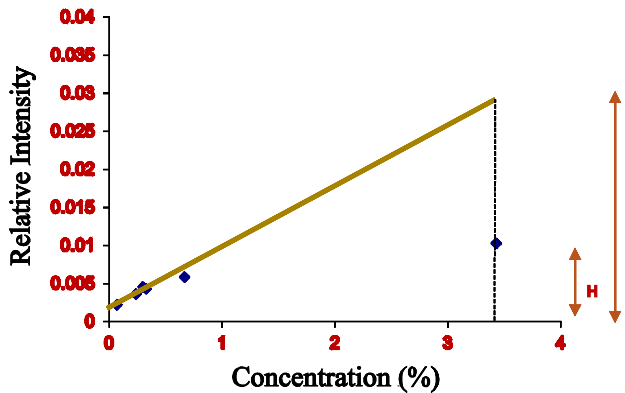
Commonly, in order to perform a quantitative analysis, an analytical calibration curve including instrument response (e.g., element signal) is depicted versus concentration (% ppm)¹ or absolute mass (gram, nanogram, etc.) [77]. Here, the characteristics of the used standard aluminums in the

¹ Parts-per-million.

Table 2 Characteristics of standard samples for construction of COG and calibration curves

Sample number	Cr (%)	Zn (%)	Mg (%)	Mn (%)	Cu (%)	Fe (%)	Si (%)
1	0.0012	0.098	0.018	0.045	0.24	0.19	0.28
2	0.004	0.029	0.65	0.225	3.43	0.582	0.895
3	0.014	0.36	1.09	1.68	0.330	0.517	0.230
4	0.011	0.020	1.16	0.24	0.07	0.18	0.097
5	0.14	4.15	4.39	0.17	0.67	0.32	0.18
6	0.073	0.18	0.25	0.070	0.30	0.75	4.550

experiment are inserted in Table 2. The calibration curves of the Cr spectral line at 427.48 nm (normalized to Al line at 305 nm) at different gas pressures are shown in Fig. 3. As it is seen, at lower pressures, i.e., <1 Torr, the calibration curve approach to a disorder situation and the error of the measurement increases. Disordination of plasma plume at very low pressure is clearly observable at 0.12 Torr. This is attributed to relatively low confinement effects of the

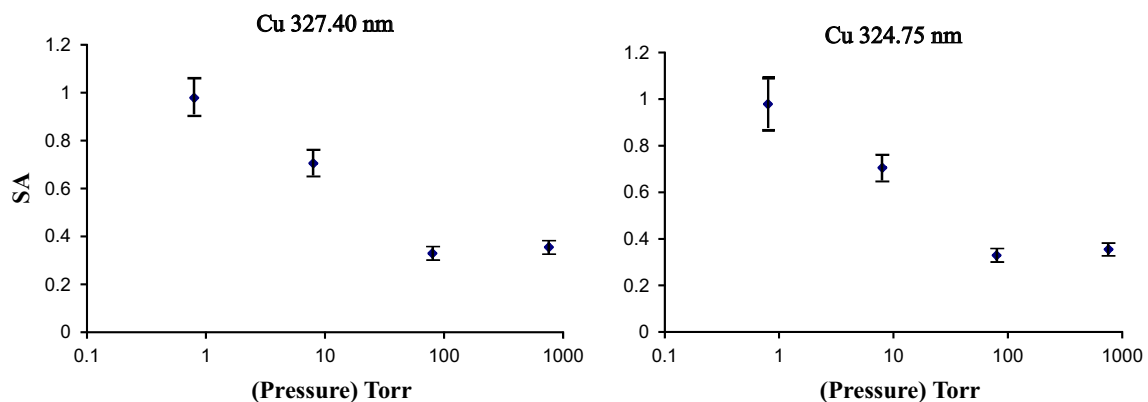
**Fig. 4** Analytical calibration curve of Cu spectral line at 324.75 nm for evaluation of self-absorption magnitude

surrounding ambient gas and much expanding of the plasma plume at few pressures. Hence, at low pressures, due to high expansion of the plasma plume toward the laser, the collisional excitation reduces and relatively dimmer plasma is created. Moreover, it can be attributed to the fact that the region selected by the collecting optics for signal acquisition is much smaller than the expanded plasma at low pressures which can causes strange behavior in calibration curve (Table 1). This behavior is in relatively good agreement with the prediction of the studies in Refs. [78, 79].

For evaluation of spectrum erosion by the calibration curve approach, the self-absorption coefficient (SA) is assessed as the ratio of self-absorbed intensity in nonlinear case (H) to the predicted spectral emission in linear condition (I) as follows:

$$SA = \frac{H}{I}. \quad (1)$$

For more illustration of the concept of the above equation, Fig. 4 shows a schematic of a calibration curve for estimation of self-absorption coefficient of relative intensity of Cu spectral line at 324.75 nm, at 1 atm pressure and at 2- μ s delay time. As it is obvious, the flattening of the calibration

**Fig. 5** Self-absorption coefficient variation of Cu spectral lines at 324.75 and 327.40 nm with pressure in logarithmic scale

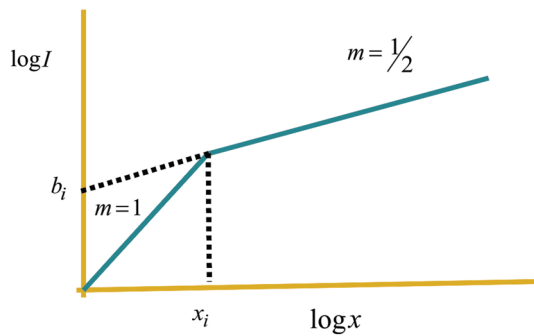


Fig. 6 Experimental curve of growth composing two slopes of 0.5 and 1 in double-logarithmic scale. (x_i, b_i) indicates the transition point from thin to thick plasma and starting of the self-absorption phenomenon

curve at high concentrations due to self-absorption phenomenon is clearly seen in this figure. Then, after analysis of the calibration curves and evaluation of self-absorption coefficients, the SA evolutions of Cu spectral lines at 324.75 and 327.40 nm with pressure are depicted in Fig. 5, in logarithmic scale. As it is clear in this figure, by increasing gas pressures for both Cu spectral lines, SA magnitude decreases, and hence, the amount of self-absorption enhances. It is attributed to the facts that at higher pressures, the plasma is more confined and more dense. The dense plasma is more optically thick because of the higher density which directly affects on the absorbing atoms number that straightly increases the amount of lines self-absorption. It should be noted that these results are qualitatively consistent with the predictions of Refs. [80, 81].

3.3 Analysis by curve of growth method

The curve of growth technique (COG) establishes a relation between spectral intensity and the plasma optical depth. Nowadays, this concept is applied in description of self-absorption phenomenon for correct quantification of spectral lines. By beginning from radiative transfer equation, the theoretical equations relating to LIBS plasma in COG model will be obtained. The details of equation derivation are fully explained in Refs. [64, 68]. According to the COG theory, at low species densities, the spectral intensity ($\text{W m}^{-2} \text{sr}^{-1}$) can be approximated by a linear function as below [64]:

$$I \cong I_p A x. \quad (2)$$

In the above equation, x is the concentration in the sample (%), I_p is Plank distribution for a black body emission ($\text{W m}^{-2} \text{sr}^{-1} \text{Hz}^{-1}$), and A equals to $A = 10^{-2} k_r N' l$, so that l is emitting area length (m), k_r is a coefficient relating to atomic absorption (m^{-1}), and N' is atom density of radiative

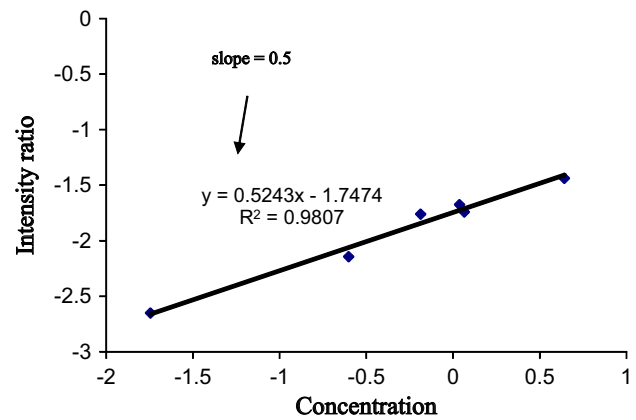


Fig. 7 Experimental COG of Mg spectral line at 280.27 nm in double-logarithmic scale

species in the plasma for the sample with 100 % concentration (m^{-3}). Furthermore, at high optical depth, the spectral intensity asymptotic behavior can be estimated as:

$$I \cong I_p [2A(\Delta\lambda_L)]^{1/2} x^{1/2}. \quad (3)$$

In the above equation, $\Delta\lambda_L$ is Lorentzian line width (m). In a double-logarithmic representation, these asymptotic equations [i.e., (2) and (3)] turn to a one linear function with slopes of 0.5 and 1 at low and high concentrations, respectively. A schematic of the experimental COG curve is depicted in Fig. 6. It should be mentioned that the concentration of transition point (from thin to thick plasma) depends on experiment condition such as laser energy and delay time. In fact, the experimental COG is the same as the calibration curve by converting it to the logarithmic scale with the slopes of 0.5 and 1. For more illustration, the experimental COG of Mg spectral line at 280.27 nm is depicted in Fig. 7. As it is clear in this figure, due to the relatively high concentration of Mg element in aluminum samples, the thick plasma condition with slope of 0.5 is satisfied in this curve and calibration curve characteristics with a slope of 1 with single linear behavior is not held for this special spectral line. Then, for the assessment of self-absorption of Cu spectral lines at 324.75 and 327.40 nm by COG technique, the variation of y -intercept of transition point (b_i) with pressure is depicted in Fig. 8. As it is seen, as the gas pressure enhances, the b_i value shifts toward the lower quantities. This refers that at higher pressures, self-absorption happens earlier and plasma moves toward thick conditions sooner than the cases of lower pressures. Consequently, the presented method tends to demonstrate that the similar results as the calibration curve technique are obtained so that higher pressures cause to increase the magnitude of self-absorption.

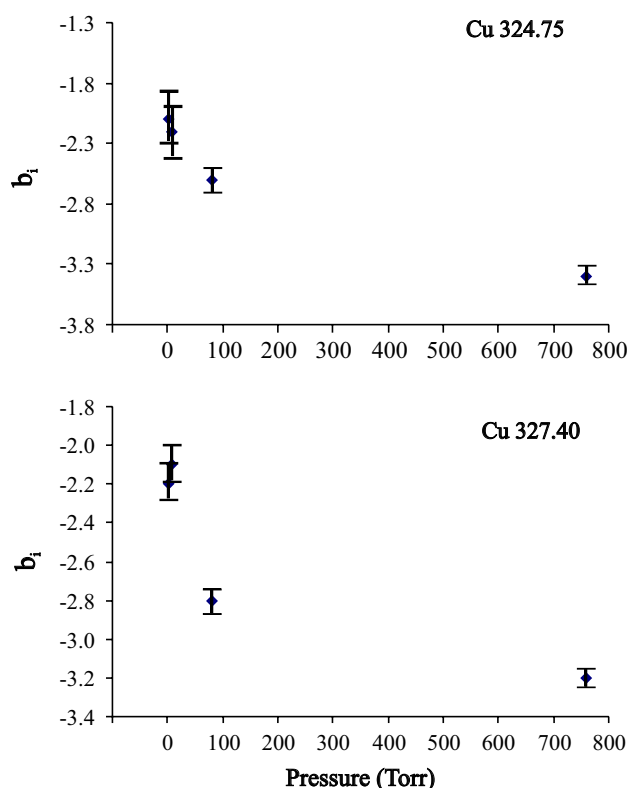


Fig. 8 Y-intercept behavior of transition point as a function of gas pressure for Cu spectral lines at 324.75 and 327.40 nm

3.4 Concentration prediction by using one standard sample

Here, a new approach of using one standard sample is presented for concentration prediction. Supplying standard samples in some situations such as biological cases is a very complicated procedure and often standard samples are not available easily. Therefore, this method can somewhat facilitate the quantitative analysis. In this paper, the introduced method explains that the calibration curve or curve of growth can be drawn by knowing the data of one point (i.e., the concentration and intensity of one standard sample) and its slope (i.e., 1 or 0.5) instead of the scattered data of different points (i.e., the various standard samples). However, it is not as accurate as the traditional calibration curve or COG, but it can be helpful for special cases like biological and geological samples. It should be mentioned that for checking the accuracy of this approach, the first sample can be selectively used for depicting the calibration curve or the curve of growth. Then, by substituting the intensities of other standard samples with known concentrations, the prediction can be performed and the accuracy of this method can be checked by comparison with their real concentrations. Therefore, by considering the slope of 1 in calibration curve and the slope of 1 or 0.5 in the

experimental curve of growth (depending on having low or high concentration), the prediction can be started. This procedure can be repeated by depicting of other COG or calibration curve by using of other single standard sample. For example, for Mg spectral line, the slope of 0.5 is approximately satisfied.

4 Conclusion

Generally, the emission characteristics of spectral lines and their erosions due to self-absorption are strongly affected by ambient gas features, i.e., the nature of the utilized gas and its pressure. So, in this paper, the influences of the He gas at different pressures on spectral self-absorption are discussed by applying two approaches: calibration curve and curve of growth. Both techniques showed the growth of spectral self-absorption by increasing the gas pressure. Furthermore, a new method of one standard sample is introduced for quantitative analysis.

Acknowledgments The authors are very thankful for Meysam Sharafkhani for his cooperation and good ideas in this work.

References

1. G. Nehrke, G. Langer, *Appl. Phys. B* **104**, 1043 (2011)
2. B. Sallé, D.A. Cremers, S. Maurice, R.C. Wiens, P. Fichet, *Spectrochim. Acta Part B* **60**, 805–815 (2005)
3. J.M. Anzano, M.A. Villoria, A. Ruíz-Medina, R.J. Lasheras, *Anal. Chim. Acta* **575**, 230–235 (2006)
4. A.K. Knight, N.L. Scherbarth, D.A. Cremers, M.J. Ferris, *Appl. Spectrosc.* **54**, 331–340 (2000)
5. M.D. Dyar, J.M. Tucker, S. Humphries, S.M. Clegg, R.C. Wiens, M.D. Lane, *Spectrochim. Acta Part B* **66**, 39–56 (2011)
6. M. Dyar, M. Carmosino, E. Breves, M. Ozanne, S. Clegg, R. Wiens, *Spectrochim. Acta Part B* **70**, 51–67 (2012)
7. J.J. Remus, J.L. Gottfried, R.S. Harmon, A. Draucker, D. Baron, R. Yohe, *Appl. Opt.* **49**, C120–C131 (2010)
8. A.M. Ollila, J. Lasue, H.E. Newsom, R.A. Multari, R.C. Wiens, S.M. Clegg, *Appl. Opt.* **51**, B130–B142 (2012)
9. S. Tzortzakis, D. Anglos, D. Gray, *Opt. Lett.* **31**, 1139–1141 (2006)
10. D. Anglos, V. Detalle, Cultural heritage applications of LIBS, in *Laser-Induced Breakdown Spectroscopy* (Springer, Berlin, 2014), pp. 531–554
11. A.W. Miziolek, V. Palleschi, I. Schechter, *Laser-Induced Breakdown Spectroscopy (LIBS)* (Cambridge University Press, Cambridge, 2006)
12. R. Grönlund, M. Lundqvist, S. Svanberg, *Opt. Lett.* **30**, 2882–2884 (2005)
13. I. Gaona, P. Lucena, J. Moros, F. Fortes, S. Guirado, J. Serrano, J. Laserna, *J. Anal. At. Spectrom.* **28**, 810–820 (2013)
14. I. Osticioli, M. Wolf, D. Anglos, *Appl. Spectrosc.* **62**, 1242–1249 (2008)
15. I. Osticioli, N. Mendes, S. Porcinai, A. Cagnini, E. Castellucci, *Anal. Bioanal. Chem.* **394**, 1033–1041 (2009)
16. L. Burgio, R.J. Clark, T. Stratoudaki, M. Doulgeridis, D. Anglos, *Appl. Spectrosc.* **54**, 463–469 (2000)

17. D. Anglos, *Analysis* **25**, 26 (2001)
18. A. Brysbaert, K. Melessanaki, D. Anglos, *J. Archaeol. Sci.* **33**, 1095–1104 (2006)
19. S. Pandhija, N. Rai, A.K. Rai, S.N. Thakur, *Appl. Phys. B* **98**, 231–241 (2010)
20. R. Wainner, R. Harmon, A. Miziolek, K. McNesby, P. French, *Spectrochim. Acta Part B* **56**, 777–793 (2001)
21. R.S. Harmon, F.C. De Lucia, A.W. Miziolek, K.L. McNesby, R.A. Walters, P.D. French, *Geochem. Explor Environ. Anal.* **5**, 21–28 (2005)
22. D.A. Cremers, M.H. Ebinger, D.D. Breshears, P.J. Unkefer, S.A. Kammerdiener, M.J. Ferris, K.M. Catlett, J.R. Brown, *J. Environ. Qual.* **30**, 2202–2206 (2001)
23. M.Z. Martin, N. Labbé, N. André, R. Harris, M. Ebinger, S.D. Wullschlegel, A.A. Vass, *Spectrochim. Acta Part B* **62**, 1426–1432 (2007)
24. G. Senesi, M. Dell’Aglio, R. Gaudioso, A. De Giacomo, C. Zacccone, O. De Pascale, T. Miano, M. Capitelli, *Environ. Res.* **109**, 413–420 (2009)
25. F.C. DeLucia Jr, A.C. Samuels, R.S. Harmon, R.A. Walters, K.L. McNesby, A. Lapointe, R.J. Winkel Jr, A.W. Miziolek, *Sens. J. IEEE* **5**, 681–689 (2005)
26. A. Galmed, A. Kassem, H. Von Bergmann, M. Harith, *Appl. Phys. B* **102**, 197 (2011)
27. R. Noll, H. Bette, A. Brysch, M. Kraushaar, I. Mönch, L. Peter, V. Sturm, *Spectrochim. Acta Part B* **56**, 637–649 (2001)
28. N.K. Rai, A. Rai, *J. Hazard. Mater.* **150**, 835–838 (2008)
29. C. Davies, H. Telle, A. Williams, *Fresenius’ J. Anal. Chem.* **355**, 895–899 (1996)
30. H. Xu, J. Bernhardt, P. Mathieu, G. Roy, S. Chin, *J. Appl. Phys.* **101**, 033124 (2007)
31. H. Imam, D. Ahmed, A. Eldakroui, *J. Appl. Phys.* **113**, 234701 (2013)
32. S. Hamzaoui, R. Khleifia, N. Jaïdane, Z.B. Lakhdar, *Lasers Med. Sci.* **26**, 79–83 (2011)
33. S. Rehse, H. Salimnia, A. Miziolek, *J. Med. Eng. Technol.* **36**, 77–89 (2012)
34. S.J. Rehse, *Biomedical applications of LIBS*, in *Laser-Induced Breakdown Spectroscopy* (Springer, Berlin, 2014), pp. 457–488
35. M. Baudelet, L. Guyon, J. Yu, J.-P. Wolf, T. Amodeo, E. Fréjafon, P. Laloi, *J. Appl. Phys.* **99**, 084701 (2006)
36. S.J. Rehse, N. Jeyasingham, J. Diedrich, S. Palchadhuri, *J. Appl. Phys.* **105**, 102034 (2009)
37. D. Rusak, B. Castle, B. Smith, J. Winefordner, *Crit. Rev. Anal. Chem.* **27**, 257 (1997)
38. R.S. Harmon, F.C. De Lucia, A. LaPointe, A.W. Miziolek, in *Defense and Security Symposium* (International Society for Optics and Photonics, 2006), pp. 62170I-62170I-62177
39. R.S. Harmon, F.C. DeLucia Jr, A. LaPointe, R.J. Winkel Jr, A.W. Miziolek, *Anal. Bioanal. Chem.* **385**, 1140–1148 (2006)
40. A. Miziolek, F.C. DeLucia, C.A. Munson, J.L. Gottfried, in *Laser Applications to Chemical, Security and Environmental Analysis* (Optical Society of America, 2008), p. LThC1
41. J.P. Singh, F.Y. Yueh, V.N. Rai, R. Harmon, S. Beaton, P. French, F.C. De Lucia Jr., B. Peterson, K.L. McNesby, A.W. Miziolek, in *Laser-Induced Breakdown Spectroscopy: Fundamental and Applications*, ed. by A.W. Miziolek, V. Palleschi, I. Schechter (Cambridge University Press, New York, 2006), pp. 368–399
42. F.C. De Lucia Jr., J.L. Gottfried, C.A. Munson, A.W. Miziolek, *Current status of standoff LIBS security applications at the United States Army Research Laboratory. Spectroscopy* **24**, 32 (2009)
43. A.W. Miziolek, F.C. De Lucia, in *SPIE Sensing Technology+ Applications* (International Society for Optics and Photonics, 2014), pp. 91010J-91010J-91010
44. R. Shu, H. Qi, G. Lv, D. Ma, Z. He, Y. Xue, *Chin. Opt. Lett.* **5**, 58–59 (2007)
45. B. Sallé, D.A. Cremers, S. Maurice, R.C. Wiens, *Spectrochim. Acta Part B* **60**, 479–490 (2005)
46. E. Vors, C. Gallou, L. Salmon, *Spectrochim. Acta Part B* **63**, 1198–1204 (2008)
47. C.A. Smith, M.A. Martinez, D.K. Veirs, D.A. Cremers, *Spectrochim. Acta Part B* **57**, 929–937 (2002)
48. W. Pietsch, A. Petit, A. Briand, *Spectrochim. Acta Part B* **53**, 751–761 (1998)
49. K.H. Kurniawan, K. Kagawa, *Appl. Spectrosc. Rev.* **41**, 99–130 (2006)
50. N. Farid, S.S. Harilal, H. Ding, A. Hassanein, *J. Appl. Phys.* **115**, 033107 (2014)
51. F. Rezaei, S.H. Tavassoli, *Spectrochim. Acta Part B* **78**, 29–36 (2012)
52. Y. Iida, *Spectrochim. Acta Part B* **45**, 1353–1367 (1990)
53. S. Khan, S. Bashir, A. Hayat, M. Khaleeq-ur-Rahman, *Phys. Plasmas* (1994-present) **20**, 073104 (2013)
54. V. Detalle, M. Sabsabi, L. St-Onge, A. Hamel, R. Héon, *Appl. Opt.* **42**, 5971–5977 (2003)
55. E. Gudimenko, V. Milosavljević, S. Daniels, *Opt. Express* **20**, 12699–12709 (2012)
56. A.J. Effenberger, J.R. Scott, *Sensors* **10**, 4907–4925 (2010)
57. M. Dawood, J. Margot, *AIP Adv.* **4**, 7111 (2014)
58. N. Farid, S. Bashir, K. Mahmood, *Phys. Scr.* **85**, 015702 (2012)
59. Y.-I. Lee, K. Song, H.-K. Cha, J.-M. Lee, M.-C. Park, G.-H. Lee, J. Sneddon, *Appl. Spectrosc.* **51**, 959–964 (1997)
60. F. Rezaei, S.H. Tavassoli, *J. Anal. At. Spectrom.* **29**, 2371–2378 (2014)
61. F. Rezaei, P. Karimi, S. Tavassoli, *Appl. Phys. B* **114**, 591–600 (2014)
62. H.-Y. Moon, K.K. Herrera, N. Omenetto, B.W. Smith, J.D. Winefordner, *Spectrochim. Acta Part B* **64**, 702–713 (2009)
63. A. El Sherbini, T.M. El Sherbini, H. Hegazy, G. Cristoforetti, S. Legnaioli, V. Palleschi, L. Pardini, A. Salvetti, E. Tognoni, *Spectrochim. Acta Part B* **60**, 1573–1579 (2005)
64. C. Aragon, J. Bengoechea, J. Aguilera, *Spectrochim. Acta Part B* **56**, 619–628 (2001)
65. C. Aragón, F. Peñalba, J. Aguilera, *Spectrochim. Acta Part B* **60**, 879–887 (2005)
66. C. Aragón, J.A. Aguilera, *Spectrochim. Acta Part B* **63**, 893–916 (2008)
67. J. Aguilera, C. Aragón, *Spectrochim. Acta Part B* **63**, 784–792 (2008)
68. J. Aguilera, J. Bengoechea, C. Aragón, *Spectrochim. Acta Part B* **58**, 221–237 (2003)
69. D. Bulajic, M. Corsi, G. Cristoforetti, S. Legnaioli, V. Palleschi, A. Salvetti, E. Tognoni, *Spectrochim. Acta Part B* **57**, 339–353 (2002)
70. L. Sun, H. Yu, *Talanta* **79**, 388–395 (2009)
71. H. Amamou, A. Bois, B. Ferhat, R. Redon, B. Rossetto, M. Ripert, *J. Quant. Spectrosc. Radiat. Transf.* **77**, 365–372 (2003)
72. H. Amamou, A. Bois, B. Ferhat, R. Redon, B. Rossetto, P. Matheron, *J. Quant. Spectrosc. Radiat. Transf.* **75**, 747–763 (2002)
73. G. Cristoforetti, E. Tognoni, *Spectrochim. Acta Part B* **79**, 63–71 (2013)
74. F. Rezaei, P. Karimi, S. Tavassoli, *Appl. Opt.* **52**, 5088–5096 (2013)
75. Y. Ralchenko, A. Kramida, J. Reader, *NIST atomic spectra database (version 4.0)* (National Institute of Standards and Technology, Gaithersburg, 2010)
76. F. Rezaei, S. Tavassoli, *Phys. Plasmas* (1994-present) **20**, 013301 (2013)

77. D.A. Cremers, F.Y. Yueh, J.P. Singh, H. Zhang, *Laser-Induced Breakdown Spectroscopy, Elemental Analysis* (Wiley, New York, 2006)
78. Ş. Yalçın, Y.Y. Tsui, R. Fedosejevs, J. Anal. At. Spectrom. **19**, 1295–1301 (2004)
79. V. Margetic, A. Pakulev, A. Stockhaus, M. Bolshov, K. Niemax, R. Hergenröder, Spectrochim. Acta Part B **55**, 1771–1785 (2000)
80. R. Brennetot, J. Lacour, E. Vors, A. Rivoallan, D. Vailhen, S. Maurice, Appl. Spectrosc. **57**, 744–752 (2003)
81. Z.A. Arp, D.A. Cremers, R.D. Harris, D.M. Oswald, G.R. Parker Jr, D.M. Wayne, Spectrochim. Acta Part B **59**, 987–999 (2004)